UDC: 535.41

Measurement of interfacial fracture parameters using coherent gradient sensing (CGS)

by **Hareesh V. Tippur** and **Li Ming Xu**, *Department of Mechanical Engineering, Auburn University, Auburn, Alabama 36849, USA*

Abstract

An optical interferometry called coherent gradient sensing (CGS) has been extended for mapping interface crack tip fields and for evaluating fracture parameters. The optical technique is a double grating shearing interferometer with an on line spatial filtering arrangement. The method offers real time full field measurements and can be used both in transmission mode and reflection mode. The interferometer measures small angular deflections of light rays which can be further related to in plane gradients of $(\sigma_x+\sigma_y)$ in transmission through elasto-optic relations. Direct interfacial crack tip measurements in a high stiffness mismatch PMMA-aluminium bimaterial system are performed. A variety of crack tip mode mixities are studied using asymmetric four point bend specimens subjected to different far field mechanical loads. The complex stress intensity factors and the associated phase angles are measured from CGS patterns using an asymptotic expansion field. The measurements are compared with finite element results.

Key Words: shearing interferometry, elasto-optic effect, crack tip fields, fringe analysis, stress intensity factors and mode mixity.

Nomenclature

I, I'	image plane intensity distribution
E_1, E_2	complex amplitude distribution
d	propagation vector
θ,λ	diffraction angle, wave length
Θ	applied load mixity
p, Δ	grating pitch and separation distance
N, N', *N, M*	fringe orders
l_1, l_2, l'_1, l'_2	geometric path lengths
$k = 2\pi/\lambda$	wave number
$\hat{\alpha}, \hat{\beta}, \hat{\gamma}$	direction cosines
e_x, e_y, e_z	unit vectors
c	elasto-optic constant
B	specimen thickness
s	offset distance
x, y	crack tip Cartesian coordinates
P	applied load
PMMA	polymethyl methacrylate
W, C, D	specimen dimensions
ε	oscillation index
ν, μ	Poisson's ratio, shear modulus
$K = K_1 + iK_2$	complex stress intensity factor
a,â	crack length and characteristic length
$\psi(a), \hat{\psi}(\hat{a})$	mode mixity
r, ϕ	crack tip polar coordinates

Introduction

Over the years different shearing interferometers have been developed and used in a wide range of engineering applications such as optical component testing, non-destructive inspection, experimental stress/strain analysis and so on[1-7]. The wave front shearing using different optical configurations has resulted in a variety of both real time and double exposure shearing interferometers. The ability of these interferometers to perform high resolution measurements using relatively simple optical set ups that are insensitive to rigid body motions and vibrations in shop floor environments have been the reason behind their popularity. Recently, a real time lateral shearing interferometer called coherent gradient sensing (CGS) has been developed for investigating quasi-static and dynamic crack growth in polymeric materials and metals[8-10]. In this investigation the usefulness of CGS is demonstrated in quantifying fracture parameters for interfacial cracks between dissimilar materials subjected to a wide range of ratios of tensile to shear tractions.

Bimaterial systems with large stiffness mismatch are commonly found in fibre reinforced composites, bonded joints, electronic packages, and so on. Failure behaviour of such systems depend on the fracture mechanics of interfaces which undergo inherently mixed mode deformations due to material property mismatch. A theoretical framework for analysing fracture of dissimilar material interfaces has been worked out in recent years[11-12]. Lately, there has been a resurgence in the interest for quantifying fracture behaviour of bimaterial systems[13-21]. They include several numerical and experimental investigations on brittle fracture of interfaces. These works primarily address bimaterial fracture mechanics issues related to crack tip deformation modelling and developing testing methods or fracture specimens for evaluating interface fracture toughness.

Asymmetric four point bend bimaterial fracture specimens are used in the current study. The crack tip parameters are obtained by full field, optical measurement of local elasto-optic effects. The interference patterns are subsequently analysed using asymptotic interface crack tip fields and fracture parameters are extracted. The present investigation takes into account non-singular stress contributions to interfacial crack tip deformations in finite size specimens by using an asymptotic expansion field. Also, interpretation of CGS fringes as derivatives and differences is discussed briefly. A relationship between the measured crack tip mixity and the applied load mixity is sought. The results

are compared with finite element calculations reported elsewhere[21].

Coherent gradient sensing (CGS)

In the following the working principle of transmission CGS is discussed and the governing equations for the method are derived. A simple interference analysis compared to the earlier ones[8-10] is presented here. The optical arrangement for transmission CGS is shown in Fig. 1 (a). It consists of a collimated beam of light propagating parallel to the optical axis. The laser beam is transmitted through a phase object in the region of interest. Subsequently, the object wave front undergoes a series of diffractions as it propagates through two Ronchi rulings G_1 and G_2 of pitch p (grating lines parallel to, say, x-axis). Note that the two grating planes are parallel and are separated by distance Δ along the optical axis. The square wave transmission profile of the gratings (chromium on glass master gratings with anti-reflection coatings have produced satisfactory results) result in a zero diffraction order and several odd diffraction orders. For the sake of simplicity consider diffraction orders E_0, E_{+1} and E_{-1} only. Here θ is the diffraction angle ($\theta \approx (\lambda/p)$). The diffracted wavefronts emerging from the grating G_2 are collected by the filtering lens and the spectral contents are displayed on the focal plane of the lens. A filtering aperture is used to block all but +1 or -1 diffraction orders as shown. The filtered information produces laterally sheared object wave fronts on the image plane. Note that the recording arrangement consisting of the lens and the camera back is kept focused on the object plane.

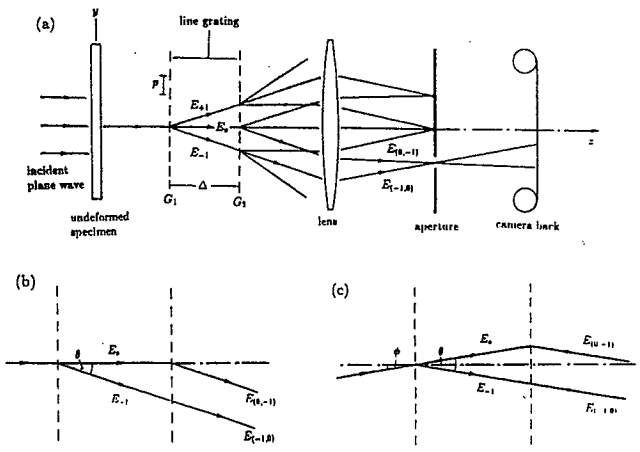

Fig. 1 (a) Optical arrangement for CGS set up, (b) Wavefront shearing for undeformed object, (c) Wavefront shearing for deformed object

Now consider the interference produced in the overlapping region of the two laterally sheared wave fronts on the image plane when the object is undeformed (Fig. 1 (b)). The path difference between E_0 and E_{-1} produces optical interference on the image plane. The total complex amplitude on the image plane is $(E_0 + E_{-1})$. The corresponding intensity distribution is,

$$I = (E_0 + E_{-1})(E_0 + E_{-1})^* = (A^2_0 + B^2_0) + 2A_0B_0 \cos[k(l_1 - l_2)] \quad (1)$$

where A_0 and B_0 are constants associated with E_0 and E_{-1}, respectively, ( )* denotes the complex conjugate, k is the wave number, and l_1 and l_2 are the path lengths of E_0 and E_{-1}, respectively, between the two gratings. The intensity represented by the above equation is a maximum when $[k(l_1 - l_2)] = 2N\pi$ where N = 0, ±1, ±2,.. ..Now, $(l_1 - l_2)$ can be expressed as,

$$(l_1 - l_2) = \Delta[1 - (\cos\theta)^{-1}] \approx \Delta[\theta^2/2] \quad (2)$$

where cos θ is expanded in the neighbourhood of zero and a second order approximation is used. Also, note that a first order approximation, cos $\theta = 1$, would result in zero optical path difference between E_0 and E_{-1}. From equations (1) and (2), for constructive interference on the image plane,

$$\theta/2 = Np/\Delta \quad (3)$$

where $k = 2\pi/\lambda$ is used. The experimental parameters can be chosen to produce a uniform bright fringe corresponding to the initial planarity of the object wavefront. Now, the above analysis can be extended for the case when the object is deformed. Consider the wavefront emerging out of a deformed object such that the propagation vector makes an angle ϕ with the optical axis (Fig. 1c). Then, the intensity of the interference pattern on the image plane is given by,

$$I' = (A^2_0 + B^2_0) + 2A_0B_0\cos[k(l'_1 - l'_2)]$$
$$\text{Here, } (l'_1 - l'_2) = \Delta[(\cos\phi)^{-1} - (\cos(\theta - \phi))^{-1}]$$
$$\approx \Delta[-\theta\phi + \theta^2/2] \quad (4)$$

where again terms smaller than ϕ^2, θ^2 and $\phi\theta$ are neglected and l'_1, l'_2 are path lengths of E_0 and E_{-1} for the deformed object. The two quantities $\theta\phi$ and $\theta^2/2$ are of the same order and hence for consistency second order approximation is used. Thus, the light intensity is a maximum when,

$$k\Delta\theta[\theta/2 - \phi] = 2N'\pi, \quad N' = 0, \pm1, \pm2, ...$$
$$[\theta/2 - \phi] = N'p/\Delta \quad (5)$$

Let the propagation vector **d** of the object wavefront be expressed as, $\mathbf{d} = \hat{\alpha}e_x + \hat{\beta}e_y + \hat{\gamma}e_z$, where $\hat{\alpha}$, $\hat{\beta}$ and $\hat{\gamma}$ are the direction cosines, and e_i be the unit normal in the ith direction. For deflections of light rays shown in Fig. 1 (c), $\hat{\alpha} = 0$, $\hat{\beta} = \sin\phi$ and $\hat{\gamma} = \cos\phi$. For small angles, $\hat{\beta} \approx \phi$. By substituting equation (3) in equation (5), gives,

$$\hat{\beta} \approx \phi = (N - N')p/\Delta \quad (6)$$

Thus, CGS provides interference patterns which represent contours of $\hat{\beta}$. The fringe order N being independent of deformation for a planar object and dependent only on the experimental parameters λ, Δ and p, one can interpret equation (6) simply as,

$$\hat{\beta} = Np/\Delta \quad (7)$$

where N = N-N' = 0, ±1, ±2..., represent fringe orders corresponding to the deviation from the initial planarity of the object wavefront. Also, the above analysis provides a basis for accounting for initial fringes (denoted by N), if any, in the event of a non-planar object wavefront or intentionally introduced carrier fringes.

In practice, optics are arranged such that initially a uniform bright field or a bright fringe is observed on the image plane when the object is underformed. Upon deformation $\hat{\beta}$ changes locally from point to point resulting in optical interference. The direction cosines can be further related to mechanical deformations as demonstrated in Tippur et al.[8] by,

$$\hat{\beta} = cB\frac{\partial(\sigma_x + \sigma_y)}{\partial y} = \frac{Np}{\Delta}; \qquad (8)$$

$$\hat{\alpha} = cB\frac{\partial(\sigma_x + \sigma_y)}{\partial x} = \frac{Mp}{\Delta}$$

where c is the elasto-optic constant for the phase object, σ_x and σ_y are plane stress components, M, N are fringe orders, and B is the nominal thickness of the specimen.

Optical mapping and fringe analysis

Specimen preparation

Symmetric four point bend bimaterial specimens are used to study interfacial crack tip fields under a wide range of mode mixities. A material combination with a relatively large stiffness mismatch consisting of PMMA (polymethylmethacrylate) and aluminium is chosen. The specimen and the loading configuration is shown in Fig. 2. The test specimens consist of two equal thickness (B = 6 mm) halves that are bonded together by a bond material consisting of methylmethacrylate monomer and a polymerising agent. Prior to bonding, the aluminium face of the interface is sand blasted to enhance bond strength. A teflon tape insert (≈50 μm thick) produces a crack like edge discontinuity of length a/W=0.33 along the interface where a is the crack length and W is the specimen height. The bond is cured at laboratory temperature prior to testing. Before testing, each specimen is optically examined in the CGS setup under no load condition to ensure that the interface is free from initial fringe patterns representing residual stresses.

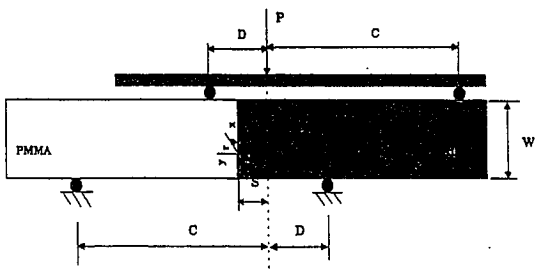

Fig. 2 Asymmetric four point bend specimen-loading configuration (negative setup)

Experiments

The bimaterial specimens are loaded in a displacement controlled loading device. Different far field mixities are introduced by varying the loading offset distance s between the interface and the loading axis (see Fig. 2). When s=0, the crack plane is subjected to pure shear. Increasing values of s result in larger moments acting on the crack plane for the same magnitude of shear force when C and D are kept constant. Also, the chosen configurations correspond to opening moment acting on the crack plane. Experiments are conducted for both positive s and negative s (+s and-s arrangements produce positive and negative shear on the crack plane, respectively). Note that the schematic in Fig. 2 corresponds to negative s configuration (net shear force on the crack plane is in the -x direction). Other relevant in plane dimensions are C/W=1.27 and D/W-0.63. The average shear and maximum normal stress acting on the crack plane are given by,

$$\tau = \frac{P}{WB}\left(\frac{C-D}{C+D}\right), \quad \sigma = 6\tau\frac{s}{W} \qquad (9)$$

From the above an applied load mixity at a point on the crack plane could be introduced as, say, $\Theta = \tan^{-1}(\tau/\sigma) = \tan^{-1}(W/6s)$. Here, Θ is dependent on the eccentricity ratio (s/W) and is independent of C and D.

A 50 mm collimated He-Ne laser beam is transmitted through the specimen in the crack tip region. The resulting fringes represent contours of $\partial(\sigma_x + \sigma_y)/\partial x$ in the PMMA half of the specimen. The interference patterns are recorded in real time for different applied loads P. Experiments are conducted using master gratings of pitch p=0.025 mm and grating separation distance Δ=50 mm. Experiments are conducted for different s/W ratios varying from-0.5 to 0.5 (or, Θ is varied between ±18° to ±90°). Typical interference patterns for two different values of s/W =-0 and +0.33 are shown in Fig. 3. The sensitivity of measurement is 0.014 degrees between successive dark and light fringes.
Considering the material above the interface ($0<\phi<\pi$), and following Rice[11], the asymptotic expression for $(\sigma_x + \sigma_y)$ is derived as,

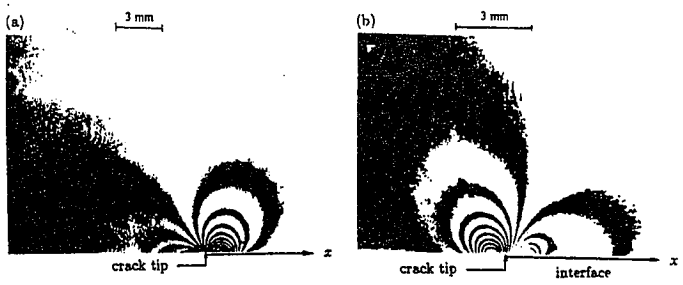

Fig. 3 Interference patterns representing contours of $\partial(\sigma_x+\sigma_y)/\partial x$ for (a) s/W=-0 (negative set up), (b) s/W=+0.33 (positive set up)

$$\frac{1}{4}(\sigma_x+\sigma_y) = \sum_{n=1,3,5...}^{\infty} e^{e(\phi-\pi)} r^{(\frac{n}{2}-1)} \times$$

$$\left\{A_n \cos[(\frac{n}{2}-1)\phi - e\ln(\frac{r}{a})]\right\} + B_n \sin[(\frac{n}{2}-1)\phi - e\ln(\frac{r}{a})]\Big\}$$

$$+\frac{2c_2}{c_1+c_2}\sum_{n=2,4,6...}^{\infty} r^{(\frac{n}{2}-1)}\left\{An\cos(\frac{n}{2}-1)\phi + Bn\sin(\frac{n}{2}-1)\phi\right\} \qquad \ldots (10)$$

For the CGS fringes mapped in this investigation, an asymptotic expression for $\partial(\sigma_x+\sigma_y)/\partial x$, can be obtained by expanding and rearranging the following expression,

$$cB\frac{\partial(\sigma_x+\sigma_y)}{\partial x}=4cB\Bigg(\sum_{n=1,3,5...}^{\infty}e^{\varepsilon(\phi-\pi)}r^{(\frac{n}{2}-2)}$$
$$\Big\{A_n\Big[(\frac{n}{2}-1)\cos((\frac{n}{2}-2)\phi-\varepsilon\ln(\frac{r}{a}))+\varepsilon\sin((\frac{n}{2}-2)\phi-\varepsilon\ln(\frac{r}{a}))\Big]$$
$$+B_n\Big[(\frac{n}{2}-1)\sin((\frac{n}{2}-2)\phi-\varepsilon\ln(\frac{r}{a}))-\varepsilon\cos((\frac{n}{2}-2)\phi-\varepsilon\ln(\frac{r}{a}))\Big]\Big\}$$
$$+\sum_{n=2,4,6,...}^{\infty}\frac{c_2}{c_1+c_2}(n-2)r^{(\frac{n}{2}-2)}\Big[A_n\cos(\frac{n}{2}-2)\phi+B_n\sin(\frac{n}{2}-2)\phi\Big]\Bigg)$$
$$=\frac{Mp}{\Delta} \qquad (11)$$

where $c_i=(\kappa_i+1)/\mu_i$, $\kappa_i=(3-\nu_i)/(1+\nu_i)$ for plane stress (i = 1 for PMMA and =2 for aluminium) and M = 0, ±1, ±2.... denote fringe orders. Here μ and ν represent shear modulus and Poisson's ratio respectively, and,

$$\varepsilon=\frac{1}{2\pi}\ln\frac{\mu_1+\mu_2\kappa_1}{\mu_2+\mu_1\kappa_2}$$

is the oscillation index. For the interface under consideration ε=0.098 for plane stress. Note that, in the above expression, the complex stress intensity factor is given by,

$$(Ka^{i\varepsilon})=2\sqrt{2\pi}\cosh(\pi\varepsilon)(A_1+iB_1)$$

and, the above asymptotic expansion reduces to its homogeneous counterpart when ε=0. The mode mixity using crack length as a scaling factor is,

$$\psi(a)=\tan^{-1}\frac{\mathrm{Im}(Ka^{i\varepsilon})}{\mathrm{Re}(Ka^{i\varepsilon})} \qquad (12)$$

The fringe patterns are digitised and, fringe location (r, ϕ) and fringe order (*M*) in the near tip region all around the crack tip is measured. Recognising the existence of a region of dominant 3-D deformations near the crack tip[20], data in the region ($r/B\geq 0.5, 30°\leq\phi\leq 150°$) near the crack tip is used in the analysis. To extract stress intensity factors from fringe patterns, one uses overdeterministic least squares data analysis. Also, in the analysis K-dominant assumptions (equation (11)) are relaxed and higher order terms are incorporated in order to account for possible non-singular contributions to the field at distances beyond the anticipated 3-D zone. The procedure consists of minimising the function $\Phi(r,\phi;A_1,B_1,A_2,B_2,....)$,

$$\Phi=\sum_{i=1}^{m}w_i[F_i-F_i^{exp}]^2 \qquad (13)$$

with respect to the constants of the series A_q and B_q (q = 1,2,3,...) resulting in a system of linear algebraic equations of the form [A]{X} = {R} where [A] is a square matrix and {R}, {X} are vectors of size equal to the number of coefficients in the asymptotic expansion. Here F and F^{exp} are the right hand sides in equation (10), m denotes the total number of data points used in the analysis and w_i are the weighting factors (assumed to be equal to 1 in the current investigation). It should be emphasised that when a large number of terms in the expansion (equation 11) are considered in the analysis, matrix [A] often tends to be ill conditioned as a result of the asymptotic nature of the fitting function. One recommends using the so called Q-R decomposition procedure[22] in view of its stability characteristics in solving such a system of equations. Traditional L-U decomposition methods often lead to unstable results in this case.

Each fringe pattern is first analysed under the assumption of K-dominance. A typical result is shown in Fig. (4a) for s/W = -0. The difference between the experimental data and the least squares fit suggests possible influence of non-singular stresses on the crack tip field and hence a need for including higher order terms in the least squares analysis. In general, details on higher order contributions such as the number of higher order terms (n) to be used in the analysis and the relative importance of each term compared to the others is unknown a priori. Therefore higher order contributions are sequentially included until the match between in the least squares fit and the data is satisfactory and, stable values of $Re(Ka^{i\varepsilon})$ and $Im(Ka^{i\varepsilon})$ are attained. For example, Fig. (4b) clearly shows an improvement in the correlation between the fit and the data when all terms up to n = 4 in equation (11) are included (or, a total of five coefficients - $Re(Ka^{i\varepsilon})$, $Im(Ka^{i\varepsilon})$, A_3, B_3, A_4) in the analysis.

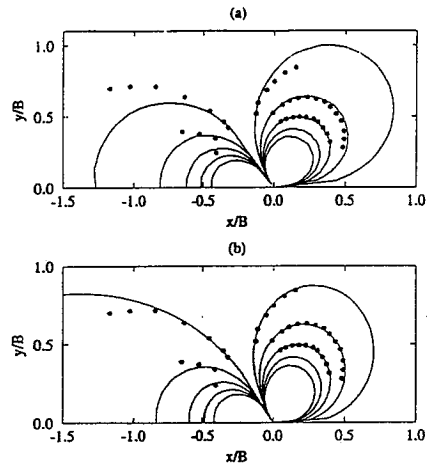

Fig. 4 Least squares analysis of interference patterns (s/W=-0), (circles are measured data and lines are least squares fit;
(a) K-dominant analysis ($Re(Ka^{i\varepsilon})$=0.43 MPa $\sqrt{m}$, $Im(Ka^{i\varepsilon})$=-0.71 MPa $\sqrt{m}$, ψ=-59°),
(b) Asymptotic field for n=4, ($Re(Ka^{i\varepsilon})$=0.50 MPa $\sqrt{m}$, $Im(Ka^{i\varepsilon})$=-0.69 MPa $\sqrt{m}$, ψ=-54°

CGS is a wave front shearing interferometric method, and it is appropriate to examine the accuracy of treating optical interference as a derivative of the quantity $(\sigma_x+\sigma_y)$. This can be done by writing the governing equations of CGS in the difference form namely,

$$cB\frac{\delta(\sigma_x+\sigma_y)}{\delta x}=\frac{Mp}{\Delta} \qquad (14)$$

where $\delta(\ )$ is the difference operator. Expressing $\delta x\approx\theta\Delta\approx(\lambda/p)$ (θ being the diffraction angle), a central difference method can be used where equation (14) takes the form,

Table-1

s/W	Difference Interpretation			Derivative Interpretation		
	No. of unknown coefficients	$\lvert(Ka^{i\varepsilon})\rvert$ MPa$\sqrt{m}$	ψ	No. of unknown coefficients	$\lvert(Ka^{i\varepsilon})\rvert$ MPa$\sqrt{m}$	ψ
-0.00	2	0.84	-60°	2	0.83	-60°
	6	0.89	-55°	5	0.85	-54°

$$cB[(\sigma_x + \sigma_y)_{i+1} - (\sigma_x + \sigma_y)_{i-1}] = M\lambda \qquad (15)$$

The left hand side of the above equation is evaluated using $r_{i\pm1} = \sqrt{\left(x_i \pm \frac{\theta\Delta}{2}\right)^2 + y_i^2}$ and $\phi_{i\pm1} = \tan^{-1}\frac{y_i}{x_i \pm \frac{\theta\Delta}{2}}$. Using the least squares procedure detailed earlier with basis functions corresponding to the asymptotic expression for $(\sigma_x + \sigma_y)$ (equation (10)), the interfacial crack tip parameters are extracted. Table 1 shows the comparison of the results based on the difference and the derivative interpretations of the crack tip fringes. Evidently, for a shearing distance of approximately 1 mm used in this investigation, both the interpretations provide reasonably close values of crack tip parameters $|Ka^{i\varepsilon}|$ and ψ.

Crack tip fracture parameters

Experimentally measured crack tip parameters Re$(Ka^{i\varepsilon})$, Im$(Ka^{i\varepsilon})$ and ψ are compared with their finite element counterparts[21] in Figs. 5-7. The variation of mixity ψ for the range $-0.5 \le s/W \le 0.5$ is shown Fig. 5. The measurements (solid boxes for negative set up and solid circles for positive setup) are in good agreement with the finite element results for both positive and negative set ups. In the range $+0 \le s/W \le +0.04$ when the applied load is dominated by shear, the measured and the computed values of crack tip mixity exceed $\pi/2$ because of a negative Re$(Ka^{i\varepsilon})$ and positive Im$(Ka^{i\varepsilon})$. As s/W increases (positive setup) ψ steadily decreases and seems to approach approximately 20° at large s/W. On the contrary, mixity corresponding to negative shear is approximately -55° at s/W =-0 and again steadily approaches 0° at large negative s/W. These observations are similar to the numerical results presented by O'Dowd, et al.,[17]. It is interesting to note that in the range of s/W ratios studied, the crack tip mixity of $\psi = 0$ has not been achieved experimentally and the specimen dimensions corresponding to larger s/W ratios could not be tested due to the space limitations in the experimental set up. However, this does not present any difficulty because symmetric three point bend or four point bend geometries could be used for the purpose.

As mentioned earlier, one could interpret s/W ratio as an applied load mixity defined by $\Theta = \tan^{-1}(\tau/\sigma)$. For the range of experimental parameters used in the study, Θ varies from approximately ±18° to ±90°. In Fig. 6, crack tip mixity ψ is plotted as a function of the nominal mixity Θ on the crack plane. The measured values of ψ are shown as the discrete data points and they clearly suggest a linear relationship with Θ ($\psi = m_o\Theta + \psi_o$). This is an observation through direct crack tip measurements demonstrating a simple

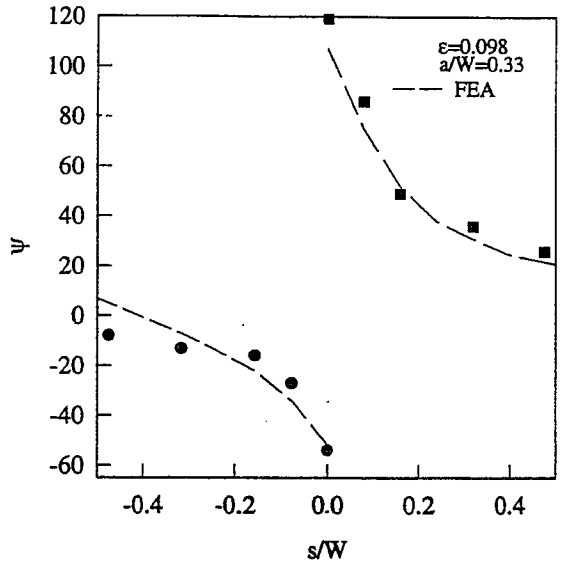

Fig 5 Comparison of optical measurement and finite element results of near tip mixity ψ for different s/W

phase shift between interfacial crack tip mixity and the applied load mixity. Such phase shifts are often suggested[12] for special cases with $\varepsilon \approx 0$ for simplifying the physical interpretation of interface stress intensity factors analogous to homogeneous counterparts. The broken line represents a straight line fit through the data whose slope m_o is approximately equal to 1 and the intercept $\psi_o \approx 18°$. Note that ψ_o is dependent on the material mismatch parameters and length scale which in this investigation is taken to be crack length a. The observed linearity in the range of s/W investigated suggests that if an alternative length scale $\hat{a} \approx 1.0 \times 10^{-3}$m is chosen instead of the current choice of a = 25 x 10^{-3}m ($\hat{a} = 1.0 \times 10^{-3}$m is one order greater than the Irwin plastic zone size estimate for PMMA), it would cause the crack tip mixity to coincide with the applied load mixity i.e., $\hat{\psi} = \Theta$ where $\hat{\psi} = \psi + \varepsilon \ln(\hat{a}/a)$. This would also simplify the interpretation of Re$(K\hat{a}^{i\varepsilon})$, Im$(K\hat{a}^{i\varepsilon})$, analogous to mixed mode stress intensity factors in homogeneous material. If one knows $\hat{a}$ *a priori* in terms of Dundur's parameters and specimen dimensions or specimen geometry, the process of measuring crack tip mixity variation can be greatly simplified. In this direction, results for simple cases such as a centrally located crack lying on a bimaterial interface subject to remote tensile and shear stresses and, crack lying along the interface of two bimaterial strips held between rigid grips subject to different grip displacements are

discussed in Hutchinson and Suo[12]. Interestingly, an estimation procedure for such a phase shift is proposed by Charalambides et al.,[19] for interfacial cracks by ignoring the singular field but considering the ratio of relative sliding of the interface to the relative opening of the interface. Their analysis suggests that the tangent of the phase shift is equal to the Poisson's ratio for plane stress conditions when large stiffness mismatch between the two materials such as the one considered here (E_1: E_2 about 20:1) exists. Based on this, for $\nu = 0.33$, the value of the phase shift is equal to 18.4° and is remarkably close to the shift observed experimentally in Fig. 6 suggesting merit in the global mode partitioning approach proposed elsewhere[19].

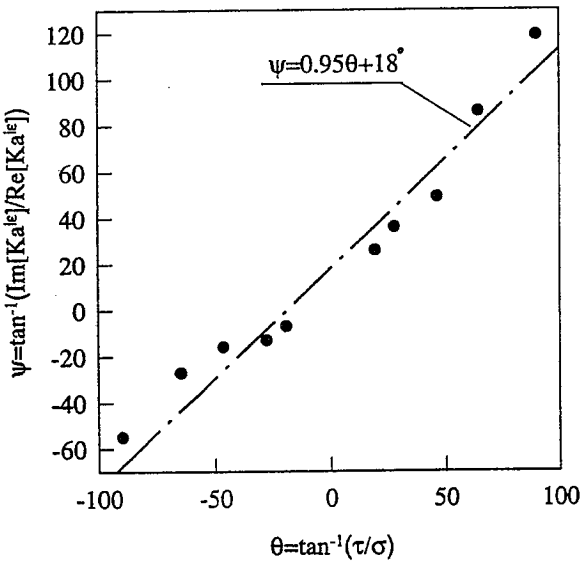

Fig. 6 Crack tip mixity ψ vs applied load mixity Θ

In Fig. 7a,b, comparison of $Re(Ka^{ie})$ and $Im(Ka^{ie})$ from experimental measurements and FEA is presented. The stress intensity factors are normalised by $(P\sqrt{a}/W^2)$. Again the two results agree well with each other. In the entire range of s/W studied, $Im(Ka^{ie})$ is relatively constant while $|Re(Ka^{ie})|$ monotonically increases with |s/W|. This is due to a con-stant shear force applied to the beam although s/W is varied. And, as discussed earlier, the measurements (Fig. 7b) estimate a negative $Re(Ka^{ie})$ when $+0 \leq s/W \leq +0.04$.

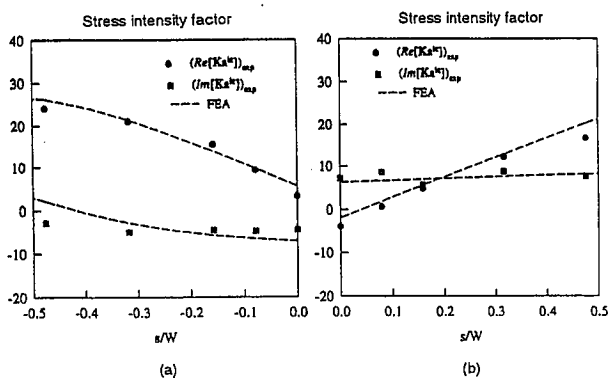

Fig. 7 Comparison of stress intensity factors obtained from optical measurements and finite element computations for different s/W; (a) negative shear, (b) positive shear

Summary and conclusions

Interface crack tip parameters namely the stress intensity factors and crack tip mixity are measured using CGS and using finite element analysis, independently. A large elastic mismatch bimaterial system consisting of PMMA and aluminium with a material mismatch parameter =0.098 is examined. Asymmetric bimaterial four point bend specimens with edge cracks cut along interfaces are studied experimentally and numerically while the applied load mixity of shear to normal stress on the interface is varied.

The technique of CGS is used for mapping crack tip fields in the PMMA half of the specimen. The crack tip parameters are extracted from the near tip interference patterns representing interface crack deformation. The contribution of non-singular stresses to the crack tip field is taken into account in the investigation by using asymptotic crack tip field expansion instead of K-dominant terms alone. This is seen to improve the experimental measurement of stress intensity factor and crack tip mixity. Complementary finite element computations were performed on identical specimens. Energy release rates were evaluated and mixities were calculated using an interaction integral method. The measured and computed results were found to be in good agreement. The crack tip mixity seems to be linearly related to the applied load mixity on the crack plane even when $\varepsilon \neq 0$.

Acknowledgments

The research is financially supported by National Science Foundation. Crack initiation and finite element modelling are detailed in a companion paper[21] while the experimental technique is emphasised here.

References

1. Murthy, M.V.R.K., "The use of a single plane parallel plate as a lateral shearing interferometer with a visible gas laser source", Applied Optics, 3, (1964), 531-534.

2. Silva, D.E., "Talbot interferometer for radial and lateral derivatives", Applied Optics, 11, (1972), 2613-2624,.

3. Hariharan, P. and Hegedus, Z.S., "Double grating interferometers II: application to collimated beams", Optics Communications, 14, (1975), 148.

4. Templeton, D.W. and Hung, Y.Y., "Shearographic fringe carrier method for data reduction computerisation", Optical Engineering, 28 (1), (1989), 30-34.

5. Shang, H.M., Toh, S.L., Chau, F.S., Shim V.W, and Tay, C.J., "Locating and sizing debonds in glassfibre reinforced plastic plates using shearography", J. Eng. Matls and Tech., 113, (1991), 99-103.

6. Patorski, K., "Shearing interferometry and the moiré method for shear strain determination", Applied Optics, 27, (16), (1988), 3567-3572.

7. Takezaki, J. and Hung, Y.Y., "Direct measurement of strains in plates by shearography", J. Applied Mechanics, 53, (1986), 125-129.

8. Tippur, H.V., Krishnaswamy, S., and Rosakis, A.J., "Optical mapping of crack tip deformations using the method of transmission and reflection CGS: A study of crack tip K-dominance", Int. J. Fract., 52, (1991), 91-117.

9. Tippur, H.V., "Coherent gradient sensing: A Fourier optic analysis and applications to fracture", Applied Optics, 31, (22), (1991), 4428-4439.

10. Tippur, H.V., and Rosakis, A.J., "Quasi-static and dynamic crack growth along bimaterial interfaces", Exp. Mech., 31, (3), (1991), 243-252,.

11. Rice, J.R., "Elastic fracture mechanics concepts for interfacial cracks", J. Appl. Mech., 55, (1988), 98-103.

12. Hutchinson J.W. and Suo, Z., "Mixed mode cracking in layered materials", Adv. in Appl. Mech., 29, (1991), 63-191.

13. Cao H.C., and Evans, A.G., "An experimental study of the fracture resistance", Mech. of Matls., (1989), 295-301.

14. Wang, J.S., and Suo, Z., "Experimental determination of interfacial toughness curves using Brazil nut sandwiches", Acta Met., 38, (7), (1990), 1279-1290.

15. Liechti, K.M., and Chai, Y.S., "Biaxial loading experiments for determining interfacial fracture toughness", J. Appl. Mech., 58, (1991), 680-687.

16. Tippur, H.V., and Ramaswamy, S., "Measurement of mixed mode fracture parameters near cracks in homogeneous and bimaterial beams", Int. J. Fract., 61, (1993), 247-265.

17. O'Dowd, N.P., Shih C.F., and Stout, M.G., "Test geometries for measuring interfacial fracture toughness", Int. J. Solids Struct., 29(5), (1992), 571-589.

18. Lu, H., and Chiang, F.P., "Photoelastic determination of SIF of an interfacial crack in a bimaterial", J. Appl. Mech., 60, (1993), 93-100.

19. Charalambides, M., Kinloch, A.J., Wang, Y., and J.G. Williams, "On the analysis of mixed mode failure", Int. J. Fract., 54, (1992), 269-291.

20. Lee, Y.J., and Rosakis, A.J., "Interfacial cracks in plates: three dimensional numerical investigation", Int. J. Solids Structures, 30 (22), (1993), 3139-3158.

21. Xu, L., and Tippur, H.V., "Fracture parameters for interfacial cracks: experimental finite element study of crack tip fields and crack initiation", AU/ME/HT Report 94/10, to appear in Int. J. Fract., (1995).

22. Dongarra, J.J., Bunch, J.R., Moler, C.B., Stewart, G.W., "LINPACK Users' Guide", SIAM, Philadelphia, USA, (1979).